



A unified PDOP evaluation method for multi-GNSS with optimization grid model and temporal–spatial resolution

Zhitao Wang^{1,2} · Shuli Song¹ · Wenhai Jiao³ · Wei Wei⁴ · Weili Zhou¹ · Guoqiang Jiao³ · Jialong Liu^{1,2}

Received: 12 July 2023 / Accepted: 7 November 2023 / Published online: 1 December 2023
© The Author(s), under exclusive licence to Springer-Verlag GmbH Germany, part of Springer Nature 2023

Abstract

Evaluation for Global Navigation Satellite System (GNSS) Position Dilution Of Precision (PDOP) is generally based on a simulated global grid with a specific Temporal–Spatial (T–S) resolution. However, the lack of a unified evaluation standard regarding the grid model, T–S resolution and evaluation period leads to inaccurate PDOP evaluation results and unreasonable comparisons among multi-GNSS. We propose the Equal-Arc-Length Grid (GRID_EAL) for PDOP evaluation, which can avoid the bias caused by uneven point distribution present in the commonly used Equal-Interval of Longitude and Latitude Grid (GRID_ELL) and provide more accurate results. Based on GRID_EAL, we thoroughly analyze the varying characteristics and convergence of PDOP metrics with different T–S resolutions. The results indicate that the optimal T–S resolution is 300 s and 3 degrees, reducing time and memory costs by 90% compared to the T–S resolution of 30 s and 3 degrees, while ensuring evaluation accuracy. Moreover, to ensure the representativity of PDOP evaluation for each system, a sliding window method is developed based on the Constellation Ground Track Repeat Period, which enables continuous daily comparisons among multi-GNSS. The proposed method satisfies the requirements for the unified evaluation standard set by the International Committee on Global Navigation Satellite Systems, International GNSS Monitoring and Assessment, and benefits PDOP evaluation and comparison for multi-GNSS.

Keywords PDOP · Service performance · Unified standard · T–S resolution · Continuous assessment and monitoring · Calculation efficiency

Introduction

Service performance of a constellation is usually determined by the geometry design and operation condition of the Global Navigation Satellite System (GNSS) (Walker 1984; Cai et al. 2009; Xue et al. 2015; Guo et al. 2019). Position Dilution Of Precision (PDOP), as one of the key parameters for evaluating constellation service performance, is related to the coefficient matrix of the observation equation, which

reflects the geometry between the user and satellites (Phillips 1984). Therefore, PDOP is generally considered a reliable reference for evaluating positioning accuracy (Sharp et al. 2009; He et al. 2014; Jiao et al. 2020), and can be used to monitor the condition of GNSS constellation. DOP is also used to aid satellite selection for multi-GNSS positioning, which can significantly improve positioning accuracy and reduce calculation time (Zhang et al. 2009). Due to the significance of PDOP in positioning and evaluating constellation service performance, various investigations and analyses related to PDOP have been conducted.

Montenbruck et al. (2013) evaluated the positioning performance of BDS-2 regional navigation satellite system. Yang et al. (2013) further evaluated the service performance of BDS-2, including metrics such as the global 95-percentile PDOP and global PDOP availability. Yang et al. (2016) focused on the service performance of GPS and BDS-2 in polar regions, analyzing the Dilution Of Precision (DOP) of these two systems. Jing et al. (2017) discussed the latitude effects on PDOP and concluded that regional navigation

✉ Shuli Song
s.song@shao.ac.cn

¹ Shanghai Astronomical Observatory, Chinese Academy of Sciences, Shanghai 200030, China

² University of Chinese Academy of Sciences, Beijing 100049, China

³ Beijing Institute of Tracking and Telecommunications Technology, Beijing 100094, China

⁴ China Satellite Navigation Office, Beijing 100000, China

systems were significantly affected by changes in latitude. Wang et al. (2019) described a method to calculate PDOP without ephemeris information and successfully predicted the performance of BDS-3. However, these researches mainly focused on individual system. Jiao et al. (2019) analyzed global PDOP for multi-GNSS over a specific time period, but only the global average PDOP for a single day has been investigated. Pan et al. (2019) analyzed global PDOP and global PDOP availability, considering different mask angles and the corresponding Constellation Ground Track Repeat Period (CGTRP) of each system. But, these PDOP evaluations were conducted using the Equal-Interval of Longitude and Latitude Grid (GRID_ELL), which existed an uneven point distribution in polar regions. Porretta et al. (2019) proposed two equal-area grids to evaluate global PDOP, aiming at improving the uneven sampling issue of GRID_ELL. Subsequently, Wang et al. (2022) employed equal-area grids for global PDOP evaluation and examined the impact of different grids on PDOP evaluation. Notably, these studies did not consider the effects caused by Temporal–Spatial (T–S) resolution of the simulated grid, and usually neglected the bias caused by GRID_ELL. Additionally, researchers applied different constraints regarding mask angle and evaluation period, leading to incomparable and insufficiently accurate results.

Currently, in the official open service Performance Standard (PS) documents of each system, a consensus has been basically reached among the four systems regarding evaluation metrics and constraints (DOD 2008, 2020b; RU 2020; CSNO 2021; EU 2021), as summarized in Table 1. The evaluation metrics for PDOP include the global average PDOP availability and the worst site PDOP availability. The constraints consist of mask angle, PDOP threshold and evaluation period length. All systems define the performance for these metrics with a mask angle of 5 degrees and a PDOP threshold of less than 6. However, the evaluation period lengths differ among the four systems, as it is generally determined based on the CGTRP. It is worth noting that while the CGTRP for Galileo is 10 sidereal days, its

evaluation period length is set to triple duration to better align with their monthly reporting requirement. In theory, using at least one complete CGTRP length can capture all the changes in PDOP worldwide during evaluations (Walker 1984; Pan et al. 2019). Therefore, the evaluation period based on at least one complete or multiple CGTRP is essential for conducting representative PDOP evaluations and constellation performance analyses.

When evaluating the PDOP metrics, it is common practice to generate a simulated global grid representing users' positions and calculate PDOP based on these grid points. Both grid model and grid T–S resolution have significant effects on evaluation results (Wang et al. 2022). However, there is currently no consensus or detailed description among systems in their respective PS documents (CSNO 2019; DOD 2020a, 2020b; RU 2020), as summarized in Table 2. Only GPS and GLONASS mentioned the grid model applied in the evaluation, and different systems employed various T–S resolutions. These varying standards make the evaluation results for different systems incomparable, and the use of improper grid models and T–S resolutions can lead to inaccurate evaluation results. To address these issues, the International Committee on Global Navigation Satellite Systems (ICG) International GNSS Monitoring and Assessment (IGMA) workgroup was established to harmonize the evaluation methods and the definitions of evaluation metrics across all systems. Its purpose is to establish a unified and reasonable evaluation standard that promotes compatibility, interoperability and transparency among all systems.

As part of the ICG IGMA work task, we aim to propose a unified method for PDOP evaluation, ensuring accurate and comparable evaluation results for all systems. The next section provides informations on the data source, the optimization evaluation method considering the various evaluation period lengths for different systems, the calculation methodology for PDOP metrics, and the generating procedure for GRID_ELL and GRID_EAL. Then, we discuss the characteristics of these two simulated grids and analyze their impacts on PDOP evaluation. Based on GRID_EAL, we determine the optimal T–S resolution, considering both evaluation accuracy and calculation cost. Additionally, the global PDOP availability and global instantaneous PDOP for

Table 1 Performance standard and constraints of PDOP evaluation metrics for the four systems

System	PDOP availability	Constraints
GPS	Global average $\geq 98\%$	Mask angle: 5°, PDOP ≤ 6 , any 24 h
	Worst site $\geq 88\%$	
BDS	Global average $\geq 98\%$	Mask angle: 5°, PDOP ≤ 6 , any 7 days
	Worst site $\geq 88\%$	
GLO	Global average $\geq 98\%$	Mask angle: 5°, PDOP ≤ 6 , any 24 h
	Worst site $\geq 84\%$	
GAL	Global average $\geq 90\%$	Mask angle: 5°, PDOP ≤ 6 , any 30 days
	Worst site $\geq 87\%$	

Table 2 Grid model and T–S resolution strategy of PDOP evaluation for the four systems

System	Grid model	T–S resolution	
		Spatial	Temporal
GPS	Equidistant spacing algorithm	4°	5 min
BDS	N/A	$\leq 1^\circ$	≤ 10 min
GLO	Based on equal-area method	1°	≤ 10 min
GAL	N/A	N/A	N/A

the four systems are validated and analyzed. Conclusions are drawn in the last section.

Data and methods

We first describe the GNSS ephemeris data used for PDOP evaluation, then propose an optimization evaluation method which enables a reasonable daily comparison of evaluation results across all systems. Calculation algorithms for PDOP metrics and grid division methods are also detailed.

Data

Three continuous periods broadcast ephemeris datasets provided by Geodetic Observatory Pecny (GOP) are used for PDOP evaluation. These datasets cover the day of year (DOY) 251–260, 261–270, and 271–280 in 2021. The evaluation period length is determined based on the CGTRP length of each system. The difference between a solar day and a sidereal day is only 236 s, which can be

ignored for PDOP evaluations (Pan et al. 2019). Therefore, the evaluation period can be simplified as one day for GPS, seven days for BDS, eight days for GLONASS, and ten days for Galileo. The details are listed in Table 3.

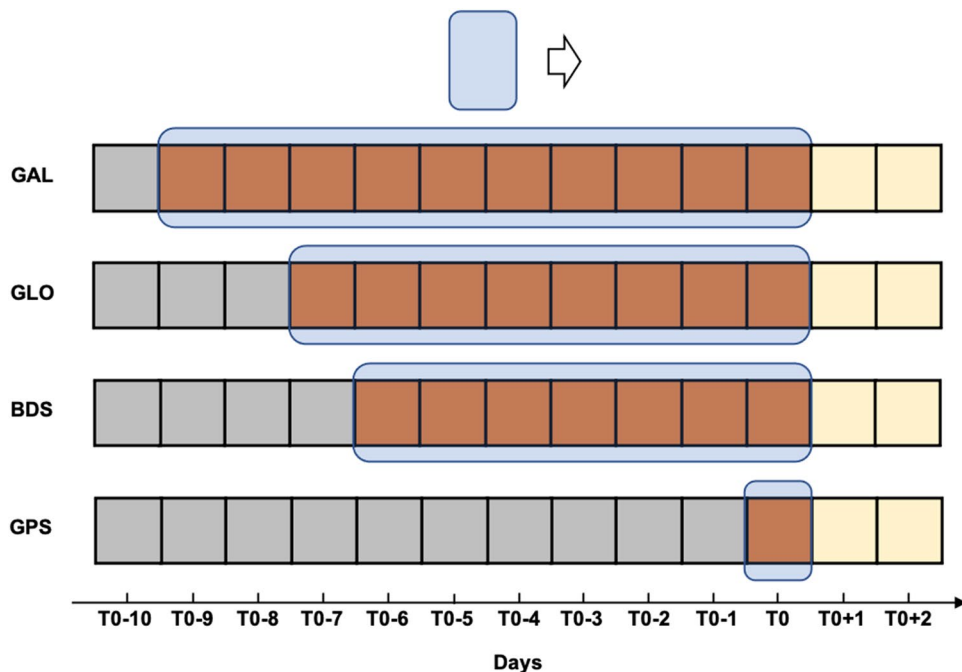
Sliding window method for the evaluation period

CGTRP length serves as a minimum requirement for obtaining evaluation results for each system, ensuring an accurate reflection of the constellation service performance. However, the variations in CGTRPs among different systems create a disparity in the number of results available over a specific evaluation period. For instance, GPS can provide ten results over a ten-day period; while, Galileo can only provide one result. This is adverse to meaningful daily comparisons among systems. To address this issue, we develop a sliding window method to ensure that representative evaluation results for all systems can be obtained daily. As shown in Fig. 1, the sliding window length for each system is set equal to its CGTRP. We can obtain the evaluation result of T0 by using the ephemeris of dates within the sliding window (e.g., for BDS it ranges from T0-6 to T0). As time passes, the sliding window moves forward by one day (e.g., for BDS it will range from T0-5 to T0+1), allowing us to continuously obtain evaluation results. This approach significantly enhances the joint evaluation capability for multi-GNSS, ensuring comparable results on a daily basis.

Table 3 Evaluation periods for the four systems (DOY for 2021)

System	Period		
	1	2	3
GPS	251	261	271
BDS	251–257	261–267	271–277
GLO	251–258	261–268	271–278
GAL	251–260	261–270	271–280

Fig. 1 Sliding window method for multi-GNSS PDOP evaluation. Different window lengths are employed to ensure that each system can obtain evaluation result based on complete CGTRP, providing an accurate representation of the system service performance



Calculation algorithms for evaluation metrics

For calculating the evaluation metrics, it is necessary to compute the PDOP values for all simulated point positions at each epoch throughout the evaluation period. The PDOP availability for all simulated point positions can be obtained through a percentage statistic. The algorithms for calculating PDOP, PDOP availability, and the final evaluation metrics are introduced as follows.

When discussing the signal-in-space service performance of a navigation constellation, the atmospheric effects on GNSS signal propagation are not taken in account. The simplified pseudorange model can be expressed as follows (Odijk 2017):

$$P_r^s = \rho_r^s + c \cdot dt_r + e \tag{1}$$

where P_r^s is the pseudorange observation between satellite s and receiver r ; ρ_r^s is the geometric distance; c is the speed of light; dt_r is the receiver clock error; and e is measurement noise.

The simplified pseudorange model can be linearized by using an initial estimated receiver position:

$$\Delta P_r^s = -e_r^s \cdot \Delta x + e \tag{2}$$

where ΔP_r^s is the observed minus computed pseudorange; $-e_r^s = -\left[\frac{E^s - E_r}{\rho_{0r}^s} \quad \frac{N^s - N_r}{\rho_{0r}^s} \quad \frac{U^s - U_r}{\rho_{0r}^s} \quad -1 \right]^T$ is the unit vector between satellite s and receiver r ; $\Delta x = [\Delta E \ \Delta N \ \Delta U \ c \cdot dt_r]$ are the four unknown elements, including the corrections of receiver coordinates in the local east-north-up frame and the equivalent distance caused by receiver clock error;

When there are n observations between satellites and a receiver, the unit vectors form an $n \times 4$ coefficient matrix A of the unknown elements. Assuming all the measurement accuracies of observations are equal and according to error propagation, the covariance of Δx can be expressed as follows:

$$Cov(\Delta X) = (A^T \cdot A)^{-1} \cdot \sigma^2 = Q \cdot \sigma^2 \tag{3}$$

where σ is the standard deviation of the observations. Q is a 4×4 matrix that is equal to the inverse of the normal matrix.

PDOP can now be calculated from the diagonal elements of matrix Q (Massatt et al. 1990; Zhu 1992):

$$PDOP = \sqrt{Q_{11} + Q_{22} + Q_{33}} \tag{4}$$

PDOP availability is defined as the percentage of the results on an observation site that meet the PDOP threshold under a specified constraint throughout a given setup period. The algorithm for computing PDOP availability is (CSNO 2019):

$$Ava_i = \frac{\sum_{t=t_{start}}^{t_{end}} \text{bool}\{PDOP_t \leq f\}}{1 + \frac{t_{end} - t_{start}}{T}} \tag{5}$$

where Ava_i is the PDOP availability of the observation site i ; T is the sampling interval; t_{start} and t_{end} are the start and end epoch; respectively, bool is the Boolean function; $PDOP_t$ is the PDOP value of the observation site at the epoch t ; and f is the PDOP threshold.

The calculation method for PDOP availability indicates that evaluation periods, represented by $t_{end} - t_{start}$, will affect the results. Therefore, it is necessary to apply at least one complete CGTRP in order to obtain a reasonable estimate of PDOP availability.

Based on simulated grid, the evaluation metrics, global average PDOP availability and the worst site PDOP availability, can be calculated:

$$\begin{cases} A_{ave} = \frac{\sum_{i=0}^N Ava_i}{N} \\ A_{wst} = \min\{Ava_i\} \end{cases} \tag{6}$$

where A_{ave} and A_{wst} are the global average PDOP availability and the worst site PDOP availability; respectively, N is the total number of global simulated grid points; and \min is the minimum value within the data group.

Grid division

GRID_ELL is commonly used due to its flexible and relatively simple modeling method. The algorithm for generating an $m \times n$ GRID_ELL is:

$$\begin{cases} \lambda = m \cdot d\lambda - \frac{\pi}{2}, \quad m \in [0, N_\lambda], \quad m \in \mathbb{Z} \\ \varphi = n \cdot d\varphi, \quad n \in [0, N_\varphi], \quad n \in \mathbb{Z} \end{cases} \tag{7}$$

where λ and φ are the latitude and longitude; respectively, $d\lambda$ and $d\varphi$ are the latitude interval and longitude interval; respectively, $N_\lambda = \pi/d\lambda$ is the latitude count, and $N_\varphi = 2\pi/d\varphi$ is the longitude count.

However, the point distribution of GRID_ELL makes it less suitable for global statistics. In contrast, GRID_EAL as an equal-area grid model can address the limitations of GRID_ELL, and the initial grid spatial resolution d is the only parameter required for generating the grid. The latitude interval and initial longitude interval can be computed as (Deserno 2004):

$$\begin{cases} N_\lambda = \frac{\pi}{d} \\ d\lambda = \frac{\pi}{N_\lambda} \end{cases} \tag{8}$$

$$d\varphi_0 = \frac{d^2}{d\lambda} \tag{9}$$

where $d\varphi_0$ is the initial longitude interval.

The point distribution for different parallels of latitude is shown in left panel of Fig. 2. On a single parallel, the point distribution is shown in right panel of Fig. 2. The longitude count $N_\varphi(\lambda)$ and the longitude interval $d_\varphi(\lambda)$ of the single parallel can be derived based on the length of the parallel and the initial longitude interval $d\varphi_0$. These two parameters are related to the latitude of parallel and can be expressed as:

$$\begin{cases} N_\varphi(\lambda) = \text{round}\left(\frac{2\pi \cdot \cos \lambda}{d\varphi_0}\right) \\ d\varphi(\lambda) = \frac{2\pi}{N_\varphi(\lambda)} \end{cases} \quad (10)$$

where round refers to rounding to the nearest whole number.

Based on (10), the latitude and longitude of grid points of GRID_EAL can be calculated as:

$$\begin{cases} \lambda = m \cdot d\lambda - \frac{\pi}{2}, m \in [0, N_\lambda], m \in \mathbb{Z} \\ \varphi = n \cdot d\varphi(\lambda), n \in [0, N_\varphi(\lambda)], n \in \mathbb{Z} \end{cases} \quad (11)$$

Grid models comparison

Based on the previous section, we can generate GRID_ELL and GRID_EAL with a spatial resolution of 5 degrees (see in Fig. 3). It can be observed that GRID_ELL does not

Fig. 2 Point distribution of GRID_EAL on parallels. The left panel shows the grid point distribution for different parallels, and the right panel shows the grid point distribution on a single parallel

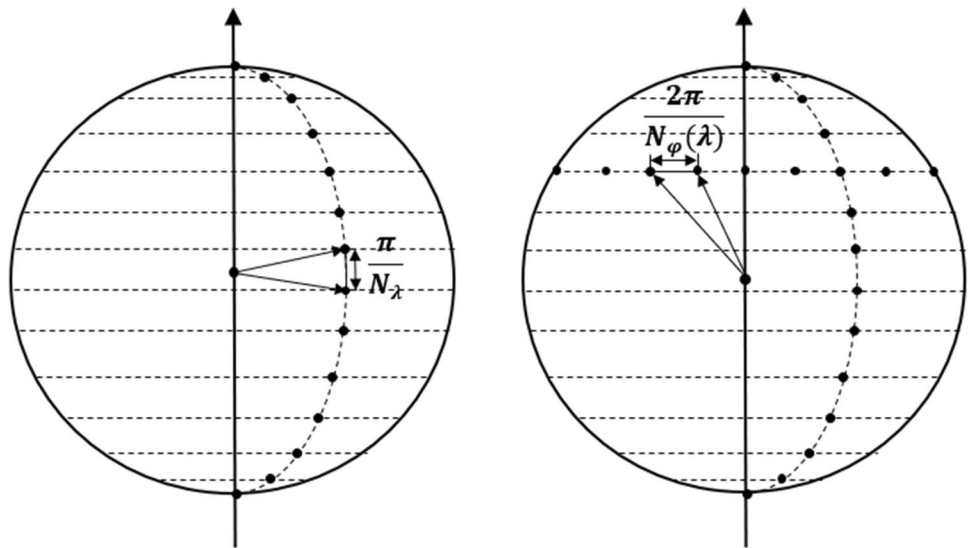
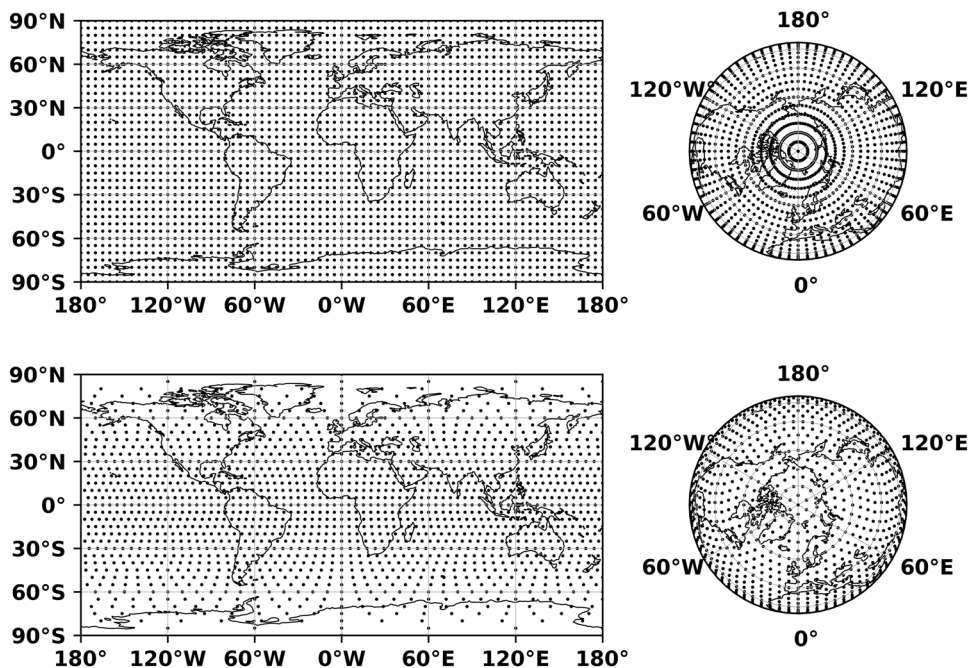


Fig. 3 Global distribution of grid points. The top panel shows the grid point distribution for GRID_ELL in the Plate Carrée projection (left) and the Orthographic projection from the earth's north polar view (right). The bottom panel shows the grid point distribution for GRID_EAL in the Plate Carrée projection (left) and the Orthographic projection from the earth's north polar view (right)



consider the actual area of different regions, leading to a significant number of redundant grid points in the earth's polar regions. Conversely, GRID_EAL based on the equal-area rule, can address this issue. Figure 4 shows the distribution of grid points across different latitude regions. For GRID_ELL, high-latitude regions contribute 60.4% of the total grid points; while, mid-latitude regions contribute only 22.1% and low-latitude regions contribute 17.5%. In the case of GRID_EAL, the corresponding percentages are 29.2% for high-latitude regions, 36.3% for mid-latitude regions, and 34.4% for low-latitude regions.

The evaluation results of PDOP metrics based on the two grid models are presented in Table 4. Considering that users typically employ a higher mask angle to enhance positioning accuracy by reducing signal noise (Teunissen et al. 2014), analyzing global PDOP with different mask angles is valuable. In this analysis, the T-S resolution is

set at 5 degrees and 600 s, and the PDOP threshold is maintained at less than 6.

It can be observed that, for GLONASS and Galileo, the differences caused by grid models are at one and two decimal places when the mask angle is 5 degrees. As the mask angle increases to 15 degrees, the differences become more significant, reaching the unit digit. For GPS and BDS, with their larger number of satellites, it is challenging to distinguish the differences when the mask angle is 5 degrees (Hein 2020). However, the differences also reach one decimal place when the mask angle is increased to 15 degrees. As the PDOP evaluation metrics are both statistical values based on the simulated grid, it reflects that GRID_EAL can efficiently avoid the bias caused by distorted point distribution, and this bias should not be neglected in evaluation.

Fig. 4 Regional distribution of grid points. Blue represents high-latitude regions (60°–90°), orange represents mid-latitude regions (30°–60°), and green represents low-latitude regions (0°–30°). The left panel corresponds to GRID_ELL; while, the right panel corresponds to GRID_EAL

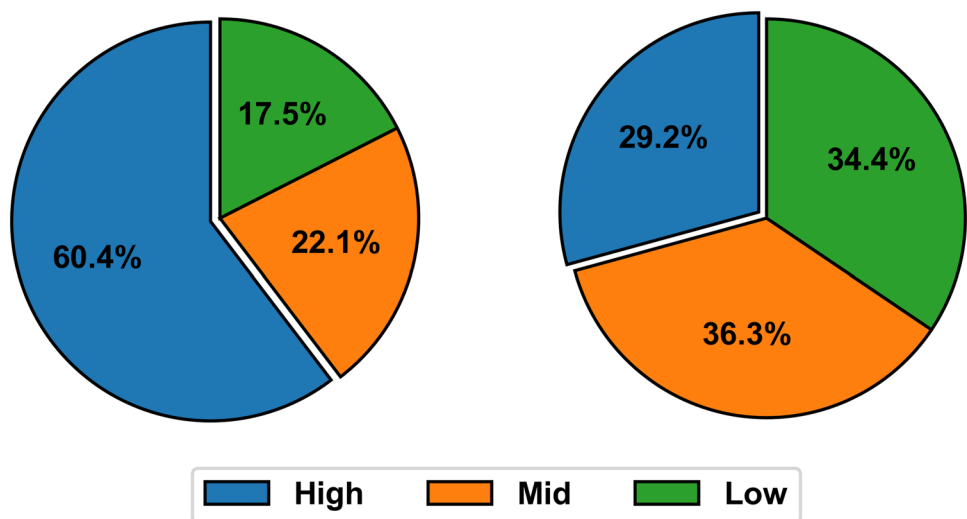


Table 4 Comparisons of PDOP evaluation metrics based on GRID_ELL and GRID_EAL. Mask angles range from 5 to 15 degrees

System	Evaluation metrics	Grid Models					
		Mask angle: 5°		Mask angle: 10°		Mask angle: 15°	
		GRID_ELL	GRID_EAL	GRID_ELL	GRID_EAL	GRID_ELL	GRID_EAL
GPS	Global average	100.000	100.000	99.942	99.950	99.514	99.512
	Worst site	100.000	100.000	97.920	97.920	95.140	95.830
BDS	Global average	100.000	100.000	99.811	99.980	99.406	99.361
	Worst site	100.000	100.000	98.785	99.110	92.364	91.766
GLONASS	Global average	99.558	99.341	96.848	95.606	88.569	84.885
	Worst site	97.915	97.830	90.103	90.277	73.090	73.004
Galileo	Global average	99.648	99.622	97.932	98.093	90.114	89.727
	Worst site	98.820	98.821	95.833	95.901	83.195	83.262

Temporal–Spatial resolution analysis

Based on the previous discussion, GRID_EAL is proposed as the grid model for PDOP evaluation. However, it is also necessary to consider the impact of T–S resolution on evaluation. Generally, higher T–S resolution leads to more accurate evaluation results, but there should be a limit. In the case of spatial resolution, the number of grid points increases rapidly after a resolution higher than 3 degrees (see in Fig. 5).

For comparing the calculation costs under various T–S resolution, an experiment is conducted based on GRID_EAL. The experiment focuses on BDS PDOP computation, with spatial resolution ranging from 1 to 8 degrees and temporal resolution ranging from 30 to 3600 s. The calculation

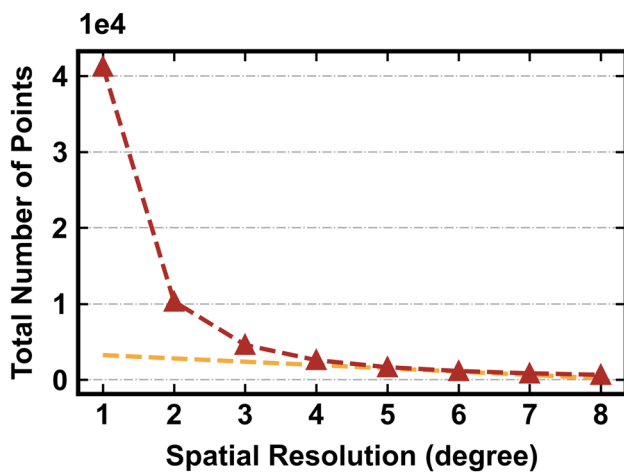


Fig. 5 Number of grid points varies as the spatial resolution increases from 1 to 8 degrees. Red line represents the changes in the number of points for GRID_EAL; while, yellow line represents the changes in the number of points at a constant rate

costs, including calculation time and memory, are listed in Table 5. It can be observed that the longest calculation time is a hundred times longer than the shortest, and the memory cost follows the same. Considering the significant impact of T–S resolution on both computation time and memory, it is crucial to determine the optimal T–S resolution that meets the accuracy requirements for evaluation while minimizing the calculation cost.

For the three different evaluation periods, the PDOP metrics for the four systems are calculated to investigate the optimal T–S resolution (see Table 3). In order to determine the optimal spatial resolution, the temporal resolution is set to 600 s, and the effects of varying spatial resolution on the PDOP metrics are examined. Since GPS and BDS have more satellites, their PDOP metrics are all close to 100 percent availability, making it challenging to discern the impact of spatial resolution. Therefore, the mask angle is set to 10 degrees for GPS and BDS and 5 degrees for GLONASS and Galileo. All results are rounded to three decimal places and presented in the Appendix. Due to the different evaluation periods, potential systematic errors exist among different periods, which makes it difficult to observe the changes in metrics caused by varying spatial resolution. Therefore, the zero-center strategy is employed:

$$\begin{cases} \text{Mean} = \frac{\sum \text{Initial_Metrics}_i}{N} \\ \text{Final_Metrics}_i = \text{Initial_Metrics}_i - \text{Mean} \end{cases} \quad (12)$$

where Initial_Metrics and Final_Metrics are the evaluation metrics before and after applying the zero-center strategy; respectively, Mean is the arithmetic mean of the metrics across different resolutions; and *i* is the resolution marker

Table 5 Calculation efficiency and memory performance for BDS PDOP computation based on GRID_EAL with different T–S resolutions. The computer hardware consists of an Intel(R) Core (TM) i9-9900 CPU @ 3.10 GHz and 64 GB RAM

Grid	T–S resolution	T–S points number	Time cost (' ")	Memory cost (Kbit)
GRID_EAL	1°, 600s	5,941,152	96'20"	67,423
GRID_EAL	2°, 600s	1,485,792	26'08"	17,429
GRID_EAL	3°, 30s	13,207,680	221'25"	159,731
GRID_EAL	3°, 60s	6,603,840	110'11"	79,812
GRID_EAL	3°, 180s	2,201,280	40'07"	26,403
GRID_EAL	3°, 300s	1,320,768	22'12"	15,778
GRID_EAL	3°, 600s	660,384	11'44"	8003
GRID_EAL	3°, 1200s	330,192	5'45"	3893
GRID_EAL	3°, 1800s	220,128	3'42"	2566
GRID_EAL	3°, 3600s	110,064	1'54"	1239
GRID_EAL	4°, 600s	372,384	6'43"	4668
GRID_EAL	5°, 600s	237,888	4'15"	3082
GRID_EAL	6°, 600s	165,312	3'02"	2215
GRID_EAL	7°, 600s	121,392	2'13"	1687
GRID_EAL	8°, 600s	93,024	1'43"	1338

(spatial resolution varies from 1 to 8 degrees, and temporal resolution varies from 30 to 3600 s).

It can be seen that worst site PDOP availability changes more obviously than global average PDOP availability as the spatial resolution varies. The change in the former reaches up to two decimal places; while, the latter reaches up to one decimal place. As shown in Fig. 6, all the results converge at the spatial resolution of 3 degrees, and this consistency is maintained across different evaluation periods.

Then the spatial resolution is set up to 3 degrees, and the effects of varying temporal resolution on the PDOP metrics are examined. The mask angle for each system remains the same as before. All results are rounded to the three decimal places and listed in Appendix. It can be observed that worst site PDOP availability is also noticeably affected by the changes in temporal resolution. Figure 7 shows the changes in PDOP metrics as temporal resolution varies based on the zero-center strategy. The results converge at 300 s, and different evaluation periods exhibit consistency.

Based on the analyses conducted, the spatial resolution of 3 degrees and the temporal resolution of 300 s are recommended as the optimal T-S resolution for PDOP

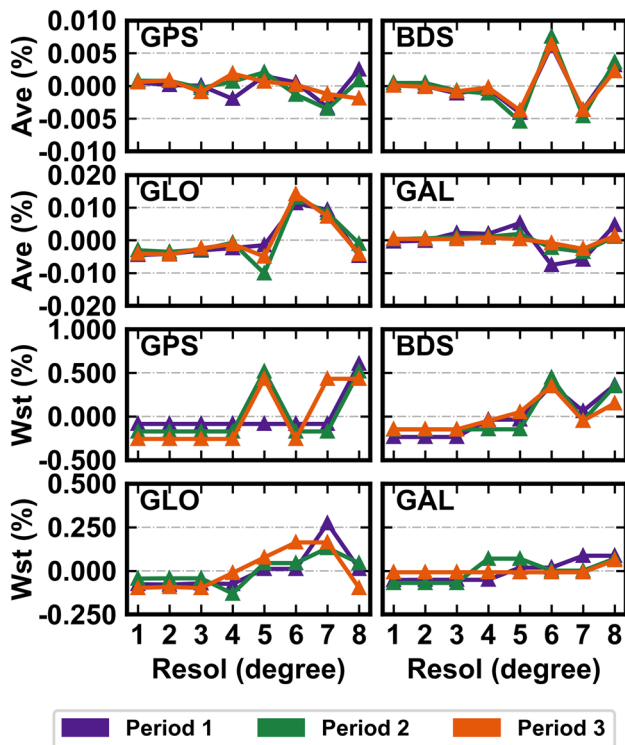


Fig. 6 Global average PDOP availability and worst site PDOP availability changes for all systems as spatial resolution varies from 1 to 8 degrees under the zero-center strategy. Ave is global average PDOP availability, and Wst is worst site PDOP availability.

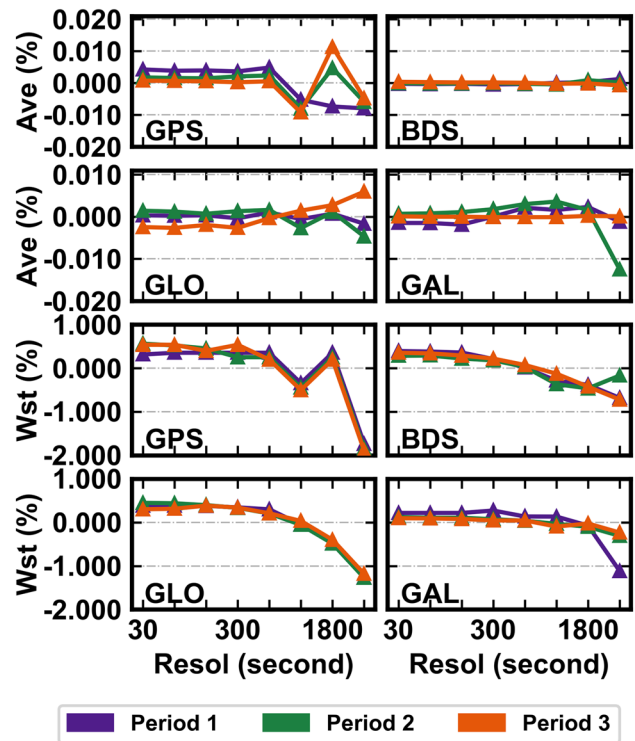


Fig. 7 Global average PDOP availability and worst site PDOP availability changes for all systems as temporal resolution varies from 30 to 3600 s (including 30 s, 60 s, 180 s, 300 s, 600 s, 1200 s, 1800s and 3600 s) under the zero-center strategy. Ave is global average PDOP availability, and Wst is worst site PDOP availability

evaluation. Higher T-S resolution has limited impact on evaluation metrics. Considering the calculation efficiency and cost analysis, the optimal T-S resolution ensures evaluation accuracy while maintaining a low calculation cost.

PDOP evaluation and application

Based on the analysis of grid models and T-S resolution, we employ the GRID_EAL with T-S resolution of 3 degrees and 300 s to evaluate PDOP. Figure 8 presents global PDOP availability for the four systems, adhering to the constraints outlined in Table 1 (mask angle: 5 degrees, PDOP threshold less than 6). For GPS and BDS, PDOP availability reaches 100% worldwide. However, for GLONASS and Galileo, PDOP availability only reaches 98% in specific areas, displaying variations across different geographical regions. GLONASS exhibits lower PDOP availability in low-latitude regions, whereas Galileo shows a noticeable decrease in mid-latitude regions.

Fig. 8 Global PDOP availability for the four systems based on GRID_EAL (spatial resolution: 3°, temporal resolution: 300 s, mask angle: 5°). Top left panel for GPS, top right panel for BDS, bottom left panel for GLONASS and bottom right panel for Galileo

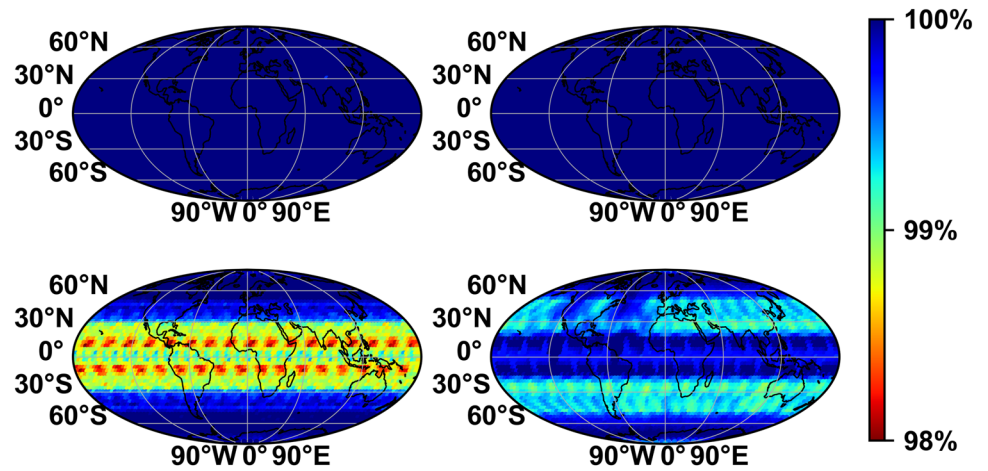


Table 6 Percentile statistics of global instantaneous PDOP for the four systems (grid model: GRID_EAL, spatial resolution: 3°, temporal resolution: 300 s, mask angle: 5°)

System	Percentile					
	50%	67%	75%	90%	95%	99%
GPS	1.568	1.658	1.743	1.955	2.106	2.298
BDS	1.351	1.523	1.615	1.884	2.018	2.372
GLO	2.058	2.284	2.395	2.907	3.359	4.529
GAL	2.019	2.254	2.383	2.864	3.172	4.459

Additionally, we also evaluate the instantaneous PDOP values for the four systems (see in Table 6), which can reflect the Single Point Positioning (SPP) accuracy when ignoring user receiver errors and propagation delays (DOD 2020b). For GPS and BDS, PDOP values are both less than 2.4 and are very close, with BDS slightly outperforming GPS except for the 99-percentile value. This suggests that BDS has better coverage in certain areas and performs slightly better than GPS; while, GPS can still provide a more even coverage worldwide. On the other hand, both GLONASS and Galileo show inferior results, with PDOP less than 4.6. However, the evaluation results are expected to be improved with the updates to GLONASS and the completion of Galileo (Hein 2020).

Conclusion

PDOP is a crucial metric to evaluate the service performance of GNSS constellations and provide a reference of positioning accuracy for users. In order to improve the evaluation accuracy and enhance comparability for multi-GNSS, we propose a unified PDOP evaluation method.

The sliding window method based on the CGTRP of each system is introduced to address the issue of various evaluation period lengths for different systems. This method ensures a representative daily evaluation and comparison for multi-GNSS, enhancing the consistency and fairness of evaluations across all systems. Based on the analysis of GRID_ELL and GRID_EAL, we propose to employ GRID_EAL for PDOP evaluation, which avoids the bias caused by uneven grid point distribution in the earth’s polar regions. This bias can reach up to 4% on PDOP availability with mask angle increasing, particularly for GLONASS and Galileo, and should not be neglected. Based on GRID_EAL, the PDOP metrics are evaluated with temporal resolution ranging from 30 to 3600 s and spatial resolution ranging from 1 to 8 degrees. The optimal T–S resolution is determined to be 300 s and 3 degrees based on the analysis of the varying characteristics and convergence of evaluation results. The results also indicate that the spatial resolution can affect two decimal places for the global average PDOP availability and one decimal place for the worst site PDOP availability at maximum, and the impact of varying temporal resolution is more significant on the evaluation metrics. Additionally, computation costs in terms of calculation

time and memory usage are evaluated using GRID_EAL with different T–S resolutions. For calculating BDS PDOP within one evaluation period, the proposed optimal T–S resolution reduces costs by 90% compared to a T–S resolution of 30 s and 3 degrees, and ensures the evaluation accuracy. Moreover, both the PDOP availability and instantaneous PDOP for the four systems are validated based on the optimization grid model and T–S resolution. The results for instantaneous PDOP indicate that the coverage of BDS has been strengthened, outperforming GPS in most areas, while GPS maintains a more even coverage compared to BDS.

ICG IGMA has accepted the unified PDOP evaluation method we proposed. This method can provide a more reliable assessment and monitoring result, promoting comparisons and interoperability for multi-GNSS.

Appendix

Results of PDOP metrics in different T–S resolutions

When the temporal resolution is fixed at 600 s, the evaluation results for the four systems are presented in Table 7, with spatial resolutions ranging from 1 to 8 degrees. The difference from mean for the four systems converges after the spatial resolution reaches 3 degrees. Subsequently, the spatial resolution is fixed at 3 degrees, the evaluation results for the four systems are presented in Table 8, with temporal resolutions ranging from 30 to 3600 s. The difference from mean for the four systems basically converges after the temporal resolution reaches 600 s.

Table 7 Comparisons of the four systems PDOP metrics in different spatial resolutions. The Mean value is calculated based on (12)

Evaluation metrics	Period	Mean	Difference from mean							
			1°	2°	3°	4°	5°	6°	7°	8°
GPS global average	1	99.948	+0.001	0.000	0.000	−0.001	+0.002	+0.001	−0.003	+0.003
	2	99.947	+0.001	+0.001	0.000	+0.001	+0.002	−0.001	−0.003	+0.001
	3	99.946	+0.001	+0.001	−0.001	+0.002	+0.001	0.000	−0.001	−0.002
GPS worst site	1	98.006	−0.086	−0.086	−0.086	−0.086	−0.086	−0.086	−0.086	+0.603
	2	98.092	−0.172	−0.172	−0.172	−0.172	+0.517	−0.172	−0.172	+0.517
	3	98.178	−0.258	−0.258	−0.258	−0.258	+0.431	−0.258	+0.431	+0.431
BDS global average	1	99.984	0.000	0.000	−0.001	0.000	−0.004	+0.006	−0.003	+0.003
	2	99.983	0.000	0.000	−0.001	−0.001	−0.005	+0.007	−0.004	+0.003
	3	99.984	0.000	0.000	−0.001	−0.000	−0.003	+0.006	−0.004	+0.002
BDS worst site	1	99.146	−0.236	−0.236	−0.236	−0.037	−0.036	+0.361	+0.061	+0.359
	2	99.157	−0.149	−0.149	−0.149	−0.149	−0.149	+0.446	−0.049	+0.347
	3	99.158	−0.148	−0.148	−0.149	−0.051	+0.049	+0.347	−0.049	+0.149
GLO global average	1	99.343	−0.005	−0.004	−0.003	−0.002	−0.002	+0.011	+0.009	−0.005
	2	99.344	−0.003	−0.004	−0.003	−0.001	−0.010	+0.013	+0.008	−0.001
	3	99.345	−0.004	−0.004	−0.002	−0.001	−0.005	+0.014	+0.007	−0.004
GLO worst site	1	97.819	−0.077	−0.079	−0.072	−0.076	+0.011	+0.011	+0.272	+0.011
	2	97.873	−0.045	−0.043	−0.043	−0.131	+0.044	+0.044	+0.130	+0.044
	3	97.841	−0.099	−0.092	−0.099	−0.013	+0.076	+0.162	+0.162	−0.099
GAL global average	1	99.616	0.000	0.000	+0.002	+0.002	+0.005	−0.008	−0.006	+0.005
	2	99.851	0.000	+0.001	+0.001	+0.001	+0.002	−0.002	−0.004	+0.001
	3	99.997	0.000	0.000	0.000	+0.001	0.000	−0.001	−0.002	+0.001
GAL worst site	1	98.803	−0.053	−0.052	−0.052	−0.052	+0.018	+0.018	+0.086	+0.086
	2	99.167	−0.070	−0.070	−0.070	−0.069	−0.069	0.000	0.000	−0.069
	3	99.871	−0.009	−0.009	−0.009	−0.009	−0.009	−0.009	−0.009	+0.060

Table 8 Comparisons of the four systems PDOP metrics in different temporal resolutions. The mean value is calculated based on (12)

Evaluation metrics	Period	Mean	Difference from mean							
			30s	60s	180s	300s	600s	1200s	1800s	3600s
GPS global average	1	99.943	+0.004	+0.004	+0.004	+0.004	+0.005	-0.005	-0.007	-0.008
	2	99.945	+0.002	+0.002	+0.001	+0.002	+0.002	-0.008	+0.005	-0.006
	3	99.945	+0.001	+0.001	+0.001	0.000	+0.001	-0.009	+0.011	-0.005
GPS worst site	1	97.566	+0.314	+0.354	+0.354	+0.354	+0.354	-0.346	+0.354	-1.736
	2	97.669	+0.561	+0.521	+0.451	+0.251	+0.251	-0.449	+0.251	-1.839
	3	97.724	+0.536	+0.536	+0.396	+0.536	+0.196	-0.504	+0.196	-1.894
BDS global average	1	99.983	0.000	0.000	0.000	0.000	0.000	0.000	0.000	+0.001
	2	99.983	0.000	0.000	0.000	0.000	0.000	0.000	+0.001	0.000
	3	99.983	0.000	0.000	0.000	0.000	0.000	0.000	0.000	-0.001
BDS worst site	1	98.897	+0.393	+0.380	+0.359	+0.210	+0.013	-0.287	-0.383	-0.684
	2	98.978	+0.283	+0.290	+0.220	+0.179	+0.030	-0.368	-0.465	-0.170
	3	98.936	+0.354	+0.340	+0.290	+0.220	+0.072	-0.128	-0.425	-0.723
GLO global average	1	99.339	0.000	0.000	0.000	0.000	+0.001	-0.001	+0.001	-0.001
	2	99.340	+0.001	+0.001	+0.001	+0.001	+0.002	-0.003	+0.001	-0.005
	3	99.343	-0.002	-0.003	-0.002	-0.003	0.000	+0.001	+0.003	+0.006
GLO worst site	1	97.617	+0.386	+0.387	+0.379	+0.344	+0.300	-0.050	-0.481	-1.265
	2	97.626	+0.448	+0.438	+0.396	+0.333	+0.204	-0.058	-0.488	-1.273
	3	97.534	+0.301	+0.313	+0.385	+0.340	+0.208	+0.033	-0.399	-1.182
GAL global average	1	99.616	-0.001	-0.001	-0.001	0.000	+0.002	+0.002	+0.002	-0.001
	2	99.849	+0.001	+0.001	+0.001	+0.002	+0.003	+0.004	+0.002	-0.013
	3	99.998	0.000	0.000	0.000	0.000	0.000	0.000	0.000	0.000
GAL worst site	1	98.616	+0.217	+0.217	+0.217	+0.272	+0.135	+0.133	-0.074	-1.117
	2	99.060	+0.121	+0.107	+0.107	+0.072	+0.037	-0.033	-0.102	-0.311
	3	99.817	+0.096	+0.092	+0.079	+0.045	+0.045	-0.095	-0.025	-0.234

Acknowledgements This study is supported by the National Natural Science Foundation of China (12073063, 12203090). The authors are grateful to ICG IGMA task force with the representatives from all institutions and the International GNSS Monitoring and Assessment System (iGMAS). The authors would like to acknowledge the International GNSS Service (IGS) and GOP for providing broadcast ephemeris.

Author contributions SS and ZW designed this research project; ZW performed the research and wrote the manuscript; SS, WH and WW gave helpful suggestions on analysis and result interpretation. GQ and WL contributed to the data analysis. GQ and JL reviewed and modified this manuscript.

Data availability The broadcast ephemeris can be accessed at ftp://ftp.pecny.cz/LDC/orbits_brd/gop3/. The datasets supporting the findings of this study are available from the corresponding authors upon request.

Declarations

Conflict of interest The authors declare no conflict of interest.

References

- Cai C, Li X, Wu H (2009) Analysis of the DOP and positioning performance of composite satellite constellation. *Sci Surv Mapp* 34(12):67–69
- CSNO (2019) Assessment method for RNSS open service performance of BeiDou navigation satellite system. China Satellite Navigation Office
- CSNO (2021) BeiDou navigation satellite system open service performance standard, Version 3.0. China Satellite Navigation Office
- Deserno M (2004) How to generate equidistributed points on the surface of a sphere. *If Polymerforschung* (Ed.) 99(2).
- DOD (2008) Global positioning system standard positioning service performance standard, 4th edn. US Department of Defense, Virginia
- DOD (2020a) Global positioning system civil monitoring performance specification, 3rd edn. US Department of Defense, Virginia
- DOD (2020b) global positioning system standard positioning service performance standard, 5th edn. US Department of Defense, Virginia

- EU (2021) European GNSS (Galileo) Open service definition document. OS SDD, Issue 1.2
- Guo S, Cai H, Meng Y, Geng C, Jia X, Mao Y, Geng T, Rao Y, Zhang H, Xie X (2019) BDS-3 RNSS technical characteristics and service performance. *Acta Geodaetica Et Cartographica Sin* 48(7):810–821. <https://doi.org/10.11947/j.AGCS.2019.20190091>
- He H, Li J, Yang Y, Xu J, Guo H, Wang A (2014) Performance assessment of single- and dual-frequency BeiDou/GPS single-epoch kinematic positioning. *GPS Solutions* 18(3):393–403. <https://doi.org/10.1007/s10291-013-0339-3>
- Hein GW (2020) Status, perspectives and trends of satellite navigation. *Satell Navig* 1(1):22. <https://doi.org/10.1186/s43020-020-00023-x>
- Jiao G, Song S, Ge Y, Su K, Liu Y (2019) Assessment of BeiDou-3 and multi-GNSS precise point positioning performance. *Sensors*. <https://doi.org/10.3390/s191112496>
- Jiao G, Song S, Liu Y, Su K, Cheng N, Wang S (2020) Analysis and assessment of BDS-2 and BDS-3 broadcast ephemeris: accuracy, the datum of broadcast clocks and its impact on single point positioning. *Remote Sens*. <https://doi.org/10.3390/rs12132081>
- Jing Y, Yang Y, Zeng A, Ming F (2017) Latitude effect in positioning performance by using BeiDou regional satellite navigation system. *Geomat Inf Sci Wuhan Univ* 42(9):1243. <https://doi.org/10.13203/j.whugis20150011>
- Massatt P, Rudnick K (1990) Geometric Formulas for Dilution of Precision Calculations. *Navigation* 37(4):379–391. <https://doi.org/10.1002/j.2161-4296.1990.tb01563.x>
- Montenbruck O, Hauschild A, Steigenberger P, Hugentobler U, Teunissen P, Nakamura S (2013) Initial assessment of the COMPASS/BeiDou-2 regional navigation satellite system. *GPS Solutions* 17(2):211–222. <https://doi.org/10.1007/s10291-012-0272-x>
- Odiijk D (2017) Positioning model. In: Peter OM, Teunissen JG (eds) *Springer handbook of global navigation satellite systems*. Springer, Berlin, pp 605–638
- Pan L, Zhang X, Li X, Li X, Lu C, Liu J, Wang Q (2019) Satellite availability and point positioning accuracy evaluation on a global scale for integration of GPS, GLONASS, BeiDou and Galileo. *Adv Space Res* 63(9):2696–2710. <https://doi.org/10.1016/j.asr.2017.07.029>
- Phillips AH (1984) Geometrical Determination of PDOP. *Navigation* 31(4):329–337. <https://doi.org/10.1002/j.2161-4296.1984.tb00883.x>
- Porretta M, Buist P (2019) Two possible grids for SVS. In: ICG IGMA and performance standards joint monthly meeting October 2019: ICG IGMA
- RU (2020) Global navigation satellite system GLONASS open service performance standard. GLONASS OS PS, Edition 2.2
- Sharp I, Kegen Y, Guo YJ (2009) GDOP analysis for positioning system design. *IEEE Trans Veh Technol* 58(7):3371–3382. <https://doi.org/10.1109/tvt.2009.2017270>
- Teunissen PJG, Odolinski R, Odiijk D (2014) Instantaneous BeiDou+GPS RTK positioning with high cut-off elevation angles. *J Geod* 88(4):335–350. <https://doi.org/10.1007/s00190-013-0686-4>
- Walker JG (1984) Satellite constellations. *J Br Interplanet Soc* 37:559
- Wang M, Wang J, Dong D, Meng L, Chen J, Wang A, Cui H (2019) Performance of BDS-3: satellite visibility and dilution of precision. *GPS Solut* 23(2):56. <https://doi.org/10.1007/s10291-019-0847-x>
- Wang Z, Song S, Jiao G, Huang C (2022) An efficient method for GNSS PDOP assessment by using equal-area grid models. *J Geod Geodyn* 42(06):606–611. <https://doi.org/10.14075/j.jgg.2022.06.010>
- Xue S, Yang Y (2015) Positioning configurations with the lowest GDOP and their classification. *J Geodesy* 89(1):49–71. <https://doi.org/10.1007/s00190-014-0760-6>
- Yang Y, Li J, Wang A, Xu J, He H, Guo H, Shen J, Dai X (2013) Preliminary assessment of the navigation and positioning performance of BeiDou regional navigation satellite system. *Sci China Earth Sci* 57(1):144–152. <https://doi.org/10.1007/s11430-013-4769-0>
- Yang Y, Xu J (2016) Navigation performance of BeiDou in polar area. *Geomat Inf Sci Wuhan Univ* 41(1):15. <https://doi.org/10.13203/j.whugis20150494>
- Zhang M, Zhang J (2009) A fast satellite selection algorithm: beyond four satellites. *IEEE J Sel Top Signal Process* 3(5):740–747. <https://doi.org/10.1109/jstsp.2009.2028381>
- Zhu J (1992) Calculation of geometric dilution of precision. *IEEE Trans Aerosp Electron Syst* 28(3):893–895

Publisher's Note Springer Nature remains neutral with regard to jurisdictional claims in published maps and institutional affiliations.

Springer Nature or its licensor (e.g. a society or other partner) holds exclusive rights to this article under a publishing agreement with the author(s) or other rightsholder(s); author self-archiving of the accepted manuscript version of this article is solely governed by the terms of such publishing agreement and applicable law.



Zhitao Wang is currently a doctoral degree candidate at Shanghai Astronomical Observatory, Chinese Academy of Sciences, Shanghai, China. His main research interests are GNSS performance assessment and marine applications.



Shuli Song is a professor at the Shanghai Astronomical Observatory, Chinese Academy of Sciences, Shanghai, China. Her main research interests are GNSS data processing and application.



Wenhai Jiao is a research fellow at the Beijing Institute of Tracking and Telecommunications Technology, Beijing, China. His main research interests are time and space coordinate references, and the overall design of GNSS.



Guoqiang Jiao received his doctoral degree at the University of Chinese Academy of Sciences, Beijing, China. His main research interests are satellite clock estimation and its applications.



Wei Wei is a senior engineer in the China Satellite Navigation Office, Beijing, China. Her main research interests are complex system intelligent control and GNSS control.



Jialong Liu is a doctoral degree candidate at the Shanghai Astronomical Observatory, Chinese Academy of Sciences, Shanghai, China. His main research interests are GNSS high-precision data processing and ionospheric activity monitoring.



Weili Zhou received her doctoral degree at the University of Chinese Academy of Sciences, Beijing, China. Her main research interests are GNSS high-precision data processing and application.